Mecánica Computacional Vol. XXI, pp. 334–346
S. R. Idelsohn, V. E. Sonzogni and A. Cardona (Eds.)
Santa Fe–Paraná, Argentina, October 2002

COMPARISON OF LINEAR AND NONLINEAR MATHEMATICAL MODELS FOR CABLES IN SIMULATION OF MOORING FORCES ON FLOATING OBJECTS

Shahrouz Aliabadi* **and Jalal Abedi†**

*Department of Engineering
223 James P. Brawley Dr., Atlanta, GA 30314, USA
Tel: 404-880-6433
Email: aliabadi@cau.edu

†Department of Engineering
223 James P. Brawley Dr., Atlanta, GA 30314, USA
Tel: 404-880-6938
Email: jabedi@cau.edu

Key Worlds: Free-Surface Flows, Mooring Forces, Finite Element Method, Fluid-Structure Interaction

Abstract. *A finite element technique is developed to compare the linear and nonlinear cable equations used in simulation of mooring forces on floating objects. In this technique, the Navier-Stokes equations for two interacting, incompressible fluids (air and water) are written and integrated over an Arbitrary Lagrangian-Eulerian domain. The interface between the air and water is tracked using a transient advection equation. The physical motions of the floating objects are handled with automatic mesh-moving schemes. The six degrees of freedom nonlinear rigid body dynamics equation are coupled with the Navier-Stokes equations to update the positions of the floating objects. The numerical example includes 3D simulations of buoyancy effects on a floating object under water constrained with a cable.*

1 INTRODUCTION

There are many marine applications involving the interaction of free-surface flows (water waves) with floating objects moored with many cables. The mooring forces are important design parameters and need to be estimated very accurately. The concentrated stresses are formed around the locations where the cables are attached to the floating objects, and therefore, subjecting these locations to a higher risk for structural failures. Advanced high performance simulation tools can be used to predict the magnitude of the mooring forces and estimate the level of stress concentrations on locations where the mooring forces act.

Computer modeling of mooring forces is complex. The partial differential equations governing the conservation of mass and momentum, commonly known as the Navier-Stokes equations, need to be coupled with the six degrees of freedom nonlinear rigid body dynamics equations to account for the position of the floating object. The tensional forces in the cables will act as a point force on the object. The magnitude and direction of these forces also need to be determined in an iterative scheme through coupling techniques with the other governing equations. In addition, the motion of the object in the computational domain needs to be addressed.

Generally, there are two distinct approaches in the numerical simulation of free-surface flows (excluding the rarely used panel method[1]). Depending on the physical characteristics of the problem, either the "moving-mesh" or the "fixed-mesh" technique is used. In the moving-mesh technique, the motion of the free-surface is absorbed by moving the computational nodes located on the free-surface.[2-3] Most of the moving-mesh techniques are based on either the space-time finite element formulations[4-5] or the solution of the governing equations over Arbitrary Lagrangian-Eulerian (ALE)[6-7] domains. In the applications where the deformation of the free-surface is large, the moving-mesh methods usually result in element distortions. As the element distortions grow and become unacceptable, the generation of a new mesh and the projection of the solution from the old mesh to the new one is essential[8]. In complex 3D applications, this procedure is extremely difficult and time consuming. In such cases, computations using fixed-mesh techniques are more desirable

The most common fixed-mesh techniques are based on the VOF[9], the level-set[10-11] and recently developed Interface-Sharpening/Global Mass Conservation (ISGMC) methods[12-13]. In these methods, the Navier-Stokes equations are solved over a non-moving mesh. A scalar function (or color function) as a marker identifies the location of the free-surface. This function is transported throughout the computational domain with a transient advection equation.

Our free-surface flow simulation techniques over fixed-meshes are based on the IS-GMC and advanced parallel computational technologies we have developed in the past several years.[14-15] These computational technologies are very user friendly and have been applied to many applications, including sloshing in tanker-trucks[2], waves interacting with marine vessels in motion,[14-15] and flow in open channels[12]. In a recent benchmark, we carried out computations using a totally unstructured mesh with more than one billion tetrahedral elements.[15] The sustained computational speed was measured at around 115 GigaFLOPS on the Cray T3E-1200

with 1024 processors. The total time spent in inter-processor communication was between 1 and 2 percent. This free-surface flow solver can produce solutions, which are highly accurate.[2,12-13,15]

The combination of the moving-mesh and fixed-mesh techniques for simulation of free-surface flows was first introduced in literature by Aliabadi et al.[16-17]. In this combination approach, the free-surface is tracked using a scalar function based on fixed-mesh techniques and the motions of the floating objects (translation and rotation) are absorbed using moving-mesh techniques. The finite element formulations for this combination approach are based on the implementation of the ISGMC in an Arbitrary Lagrangian-Eulerian (ALE) moving-mesh domain. We refer to this combination method as MM-ISGMC. The MM-ISGMC method is applied to complex 3D problems involving the free-surface flows interacting with objects in motion.[16-17]

Recently, we have developed a fluid-structure interaction simulator by incorporating the effect of cables into the MM-ISGMC. In this article, we describe and compare two mathematical models for cables. In the linear model, we assume that the cables act as linear springs subjected to tensional forces (no resistance to the compression force). In the nonlinear model, we use the transient, nonlinear finite element formulation derived from the principal of virtual work. The comparisons between these two models in the simulation of mooring forces are the main scope of this article.

The governing equations and the finite element formulations are described in Section 2. The iterative solution strategy is briefly discussed in Section 3. The numerical example and results are provided in Section 4 following the concluding remarks in Section 5.

2 GOVERNING EQUATIONS AND FINITE ELEMENT FORMULATIONS

We consider the governing equations for two interacting fluids in the spatial domain Ω and its boundary Γ. Here we assume that the spatial domain and its boundary are both functions of time, *t*. The two fluids are incompressible (e.g. air-water) and separated with an interface. Along the interface, the traction force is continuous (surface tension is negligible). The governing equations of two fluids are the Navier-Stokes equations written in the Arbitrary Lagrangian-Eulerian (ALE) domain. These equations are:

$$\rho\left[\left.\frac{\partial \mathbf{u}}{\partial t}\right|_{\xi} + (\mathbf{u}-\mathbf{u}_{mesh})\cdot\nabla\mathbf{u}-\mathbf{g}\right]-\nabla\cdot\boldsymbol{\sigma}=0 \tag{1}$$

$$\nabla\cdot\mathbf{u}=0 \tag{2}$$

where

$$\boldsymbol{\sigma} = -\mathrm{p}\,\mathbf{I} + 2\mu\boldsymbol{\varepsilon}(\mathbf{u}),$$

$$\boldsymbol{\varepsilon} = \frac{1}{2}(\boldsymbol{\nabla}\mathbf{u} + \boldsymbol{\nabla}\mathbf{u}^{\mathrm{T}}). \tag{3}$$

Here $\mathbf{u}$, $\mathbf{u}_{mesh}$, p, ρ, $\mathbf{g}$, and μ are the fluid velocity, mesh velocity, pressure, density, gravitational force, and dynamic viscosity, respectively. The strain tensor is denoted by $\boldsymbol{\varepsilon}$ and $\mathbf{I}$ represents the identity tensor. Equations (1-2) are completed by an appropriate set of boundary and initial conditions. The stabilized finite element formulations for equations (1-2) are written as:

$$\begin{aligned}
&\int_{\Omega} \mathbf{w}^h \cdot \rho[\frac{\partial \mathbf{u}^h}{\partial t} + (\mathbf{u}^h - \mathbf{u}^h_{mesh}) \cdot \boldsymbol{\nabla}\mathbf{u}^h - \mathbf{g}]d\Omega + \int_{\Omega} \boldsymbol{\varepsilon}(\mathbf{w}^h) : \boldsymbol{\sigma}(p^h, \mathbf{u}^h)d\Omega \\
&+ \int_{\Omega} q_p^h \boldsymbol{\nabla}\cdot\mathbf{u}^h d\Omega + \sum_{e=1}^{ne} \int_{\Omega^e} \frac{\tau_m}{\rho}\left[\rho(\mathbf{u}^h - \mathbf{u}^h_{mesh})\cdot\boldsymbol{\nabla}\mathbf{w}^h - \boldsymbol{\nabla}\cdot\boldsymbol{\sigma}(q_p^h, \mathbf{w}^h)\right]\cdot \\
&\left[\rho[\frac{\partial \mathbf{u}^h}{\partial t} + (\mathbf{u}^h - \mathbf{u}^h_{mesh})\cdot\boldsymbol{\nabla}\mathbf{u}^h - \mathbf{g}] - \boldsymbol{\nabla}\cdot\boldsymbol{\sigma}(p^h, \mathbf{u}^h)\right]d\Omega \\
&+ \sum_{e=1}^{ne} \int_{\Omega^e} \tau_c \boldsymbol{\nabla}\cdot\mathbf{w}^h \rho \boldsymbol{\nabla}\cdot\mathbf{u}^h d\Omega = \int_{\Gamma_{h_u}} \mathbf{w}^h \cdot \mathbf{h}\, d\Gamma.
\end{aligned} \tag{4}$$

Here, $\mathbf{w}$ and q are linear test functions for the velocity and pressure, respectively. In this formulation, the first three integrals together with the right hand side term are the Galerkin finite element formulation. The first element-level integral includes the stabilizations [2]. The second element-level integral is the least-square stabilization of the continuity equation, which enhanced the robustness of the finite element formulation at high Reynolds numbers. The details of the stabilization techniques and the definitions of the coefficients τ_m and τ_c, can be found in [2,5,12,18-19].

The interface function, ϕ, has two distinct values (0,1) and is used to differentiate between the two fluids. A transient advection equation transports this function throughout the computational domain with the fluid velocity as:

$$\left.\frac{\partial\phi}{\partial t}\right|_{\xi} + (\mathbf{u} - \mathbf{u}_{mesh})\cdot\boldsymbol{\nabla}\phi = 0. \tag{5}$$

Using ϕ, the density and viscosity can be calculate as:

$$\rho = \phi\rho_A + (1-\phi)\rho_B\,,$$
$$\mu = \phi\mu_A + (1-\phi)\mu_B\,, \tag{6}$$

where the subscripts *A* and *B* denote the fluid *A* and fluid *B*. The artificial diffusion finite element formulation for Equation (5) leads to:

$$\int_\Omega \psi^h \left[\frac{\partial \phi^h}{\partial t} + (\mathbf{u}^h - \mathbf{u}^h_{mesh}) \cdot \nabla \phi^h \right] d\Omega + \sum_{e=1}^{ne} \int_{\Omega^e} \tau_i \nabla \psi^h \cdot \nabla \phi^h d\Omega = 0\,, \tag{7}$$

where ψ is a linear test function for the interface function. Here the first integral is the Galerkin finite element formulation and the second integral is the artificial diffusion stabilization. The artificial diffusion stabilization technique is used for over stabilization.[2,12] This feature allows us to enforce the conservation of mass not only locally, but also globally. In the IS-GMS, the sharpness of the interface function is recovered after each nonlinear iteration.[12-13,17]

There is no limit on the number of cables, which can be attached to the floating objects. For nonlinear hawsers, the equation governing the dynamics of the nonlinear cables can be written as:

$$\rho_c \left(\frac{\partial^2 \mathbf{x}}{\partial t^2} - \mathbf{g} \right) = \nabla \cdot \mathbf{T} \tag{8}$$

$$\mathbf{x}\big|_{t=0} = \mathbf{X}\,,$$
$$\left.\frac{\partial \mathbf{x}}{\partial t}\right|_{t=0} = 0\,, \tag{9}$$

where $\mathbf{x}$ is the position vector, $\mathbf{X}$ is the initial position, ρ_c is the cable density, and $\mathbf{T}$ is the Cauchy stress tensor. Locally, the Green strain tensor has only one component, which can be defined as:

$$\mathbf{E}_{11} = \frac{1}{2}\left(\left\| \frac{\partial \mathbf{x}}{\partial s} \right\|^2 - \left\| \frac{\partial \mathbf{X}}{\partial s} \right\|^2 \right), \tag{10}$$

where s is a tangent vector in the original configuration of the cables. The Cauchy stress tensor, **T,** and the 2nd Piola-Kirchoff stress tensor, **S,** are related through geometry deformation. Under the assumption of small strain, but large geometry displacements, the only component of **S** in the s direction is:

$$\mathbf{S}_{11} = E_c \, \mathbf{E}_{11} \tag{11}$$

Here E_c is the Young's modulus of elasticity of the cable. The finite element formulation for Equation (8) is derived from the principle of virtual work [20] leading to:

$$\rho_c \int_{\Gamma_0} \mathbf{H}^h \cdot \left(\frac{\partial^2 \mathbf{x}^h}{\partial t^2} + \theta \frac{\partial \mathbf{x}^h}{\partial t} - \mathbf{g} \right) d\Gamma + \frac{1}{2} E_c \int_{\Gamma_0} \left(\left\| \frac{\partial \mathbf{x}}{\partial s} \right\|^2 - \left\| \frac{\partial \mathbf{X}}{\partial s} \right\|^2 \right) \frac{\partial \mathbf{H}}{\partial s} \cdot \frac{\partial \mathbf{x}}{\partial s} d\Gamma = 0, \tag{12}$$

where **H** is the test function for hawser displacements. Here we assume that the fluid does not affect the cable motion directly. Instead, a numerical damping, θ, is introduced to dampen the oscillations in time. In this formulation, all of the integrations are carried out in the original domain rather than current deformed domain.

For the linear model, we have:

$$\mathbf{S}_{11} = E_c \frac{< L_f\text{-}L_i >}{L_i},$$

$$< L_f\text{-}L_i >= \begin{cases} L_f\text{-}L_i & L_f > L_i \\ 0 & L_f < L_i \end{cases}. \tag{13}$$

Here, L_f and L_i are the final and initial length of the cable, respectively.

The motions of the floating objects are handled using an automatic mesh moving scheme. In our mesh-moving scheme, the mesh connectivity does not change as the nodes are moved to the new locations. Here, we assume that the computational domain is made of elastic material[8]. We solve linear elasticity equations to obtain the displacements for every computational node. These equations are:

$$\nabla . \left[\lambda_1 (\nabla . \mathbf{d}) \mathbf{I} + 2\lambda_2 \nabla \boldsymbol{\kappa}(\mathbf{d}) \right] = \mathbf{0} ,$$

$$\boldsymbol{\kappa} = \frac{1}{2} (\nabla \mathbf{d} + \nabla \mathbf{d}^{\mathrm{T}}) , \tag{14}$$

where $\mathbf{d}$ is the displacement, $\boldsymbol{\kappa}$ is the strain tensor, and λ_1 and λ_2 are the linear elasticity coefficients. The finite element formulation for these equations is the Galerkin formulation written as:

$$\int_{\Omega} \boldsymbol{\kappa}(\boldsymbol{\pi}^h) : \left[\lambda_1 (\nabla . \mathbf{d}^h) \mathbf{I} + 2\lambda_2 \nabla \boldsymbol{\kappa}(\mathbf{d}^h) \right] d\Omega = 0 , \tag{15}$$

where $\boldsymbol{\pi}$ is the test function for the displacements.

The six degrees of freedom nonlinear rigid body dynamics are solved to locate the new position and orientation of the floating objects. Here we consider two coordinate systems, one attached to the computational domain, X, and the other attached to the floating object, Y. The rotation matrix, $\mathbf{Q}$, transfers components of any arbitrary vector from the X coordinate system to the Y coordinate system. The nonlinear rigid body dynamics equations for the center of gravity of the object are:

$$\mathbf{F}_{\mathrm{X}} - m \mathbf{g}_{\mathrm{X}} = m \mathbf{a}_{\mathrm{X}} , \tag{16}$$

$$\mathbf{M}_{\mathrm{X}} = [\mathbf{Q}^T \mathbf{J}_{\mathrm{Y}} \mathbf{Q}] \boldsymbol{\alpha}_{\mathrm{Y}} , \tag{17}$$

where $\mathbf{F}_{\mathrm{X}}$ and $\mathbf{M}_{\mathrm{Y}}$ are the total force and angular momentum exerted on the center of gravity of the object by the fluids, respectively. The linear and angular accelerations are $\mathbf{a}_{\mathrm{X}}$ and $\boldsymbol{\alpha}_{\mathrm{Y}}$. The mass of the object is m and its moment of inertia is $\mathbf{J}_{\mathrm{Y}}$. Here the subscribed "X" and "Y" denotes the coordinate system where the components of the vectors and matrices are evaluated.

3 ITERATIVE SOLUTION STRATEGY

The discretization of the finite element formulations results in a series of coupled, nonlinear systems of equations that need to be solved at every time step. The nonlinear system of equations in vector form can be written as:

$$\mathrm{F}(\dot{\mathbf{s}}, \mathbf{s}) = \mathrm{L}, \tag{18}$$

where the vector $\mathbf{F}$ is the function of nodal unknowns, $\mathbf{s}$, and its time derivative, $\dot{\mathbf{s}}$. Here $\mathbf{L}$ is the known right-hand-side vector. After linearization using the Newton-Raphson algorithm, we need to solve a series of first order linear differential equation systems. These systems are also solved iteratively using the GMRES update algorithm[18,21]. For very large systems of equations, we use a matrix-free iteration strategy[18]. This element-vector-based computation totally eliminates the need to form any matrices, even at the element-level.

4 NUMERICAL EXAMPLE

4.1 Buoyancy effect on floating object under water

Here we simulate the buoyancy effect on a cubic object completely under water. The nondimensional computational domain covers a volume $-0.25 \le x \le 4.0$, $0.0 \le y \le 1.25$, $-0.75 \le z \le 0.75$, and the cubic object covers a volume of $1.5 \le x \le 2.5$, $0.35 \le y \le 0.65$, $-0.25 \le z \le 0.25$. The density of the cubic object is half that of water. The water elevation (in y direction) is 0.75. A single hawser is attached at one end to the ground at point $\mathrm{A}(0.0, 0.0, 0.0)$ and at the other end to point $\mathrm{B}(1.5, 0.35, 0.0)$ located on the object. The density of the cable is 1.5 times the density of water. This is a relatively light cable. Since the cable remains completely under water, the effective density of the cable is half of the water (due to buoyancy forces). The nondimensional Young's modulus of elasticity and the cross-section area of the cable are 1000 and 0.001, respectively.

The simulations are carried out using two finite element meshes. The coarse mesh has 199,666 nodes and 1,214,076 tetrahedral elements. The fine mesh is obtained by simply subdividing each element of the coarse mesh into 8 elements. The cable is modeled using both Equation (8) (nonlinear) and Equation (13) (linear). Here we present 4 solutions labeled as *Nonlinear-Coarse* for coarse mesh using Equation (8), *Linear-Coarse*, for coarse mesh using Equation (13), *Nonlinear-Fine* for fine mesh using Equation (8) and *Linear-Fine* for fine mesh using Equation (13). For the nonlinear model, the cable is discretized using 20 elements.

Initially, we assume that the hawser is stress-free and completely straight, connected from point A to point B. As the cubic object rises to the free-surface of water, tensional force is generated in the cable, which causes the floating object to move toward left (-x direction) and slightly rotate counterclockwise. The simulations are carried out on the Cray T3E with 64

processors. For both meshes, the time step is 0.005 and the total number of time steps is 400. In the coarse mesh simulations, the number of nonlinear iterations per time step is 4 and the Krylov subspace in the GMRES is 40. In the fine mesh simulations, 5 nonlinear iterations are performed at each time step and the Krylov subspace in the GMRES is set to 50.

Figure 1 shows the position of the cable at times equal to 0.5 and 1.0. In this figure, the graphs on the left and right sides correspond to coarse mesh and fine mesh, respectively. The difference between the solutions obtained using both meshes is small. From these graphs, we can also see that the linear and nonlinear models for the cables result in almost identical solutions. However, the differences between the solutions of these two models can be seen in Figure 2. In this figure, the tensional forces for all four solutions are plotted versus time. As we can see, the difference between the linear and nonlinear models can be as high as 15% in tensional forces. Also, the solutions for the nonlinear cable model show two pull-relax scenarios whereas the linear model experience only one. Figure 3 shows the cross-section of the solution at $z = 0.0$ and for times at 0.1 and 2.1 (top and bottom). Here, the color shows the water and air (green for air and red for water) for the *Nonlinear-Fine* solution. In this figure, we can clearly see that the water is still drifting off of the floating object into the tank. Our simulation model is capable of separating part of the water and re-merging it. Since the set of solutions using the coarse and fine meshes for two different cases (linear and nonlinear models) are very similar, we can conclude that the simulation results are reasonably accurate.

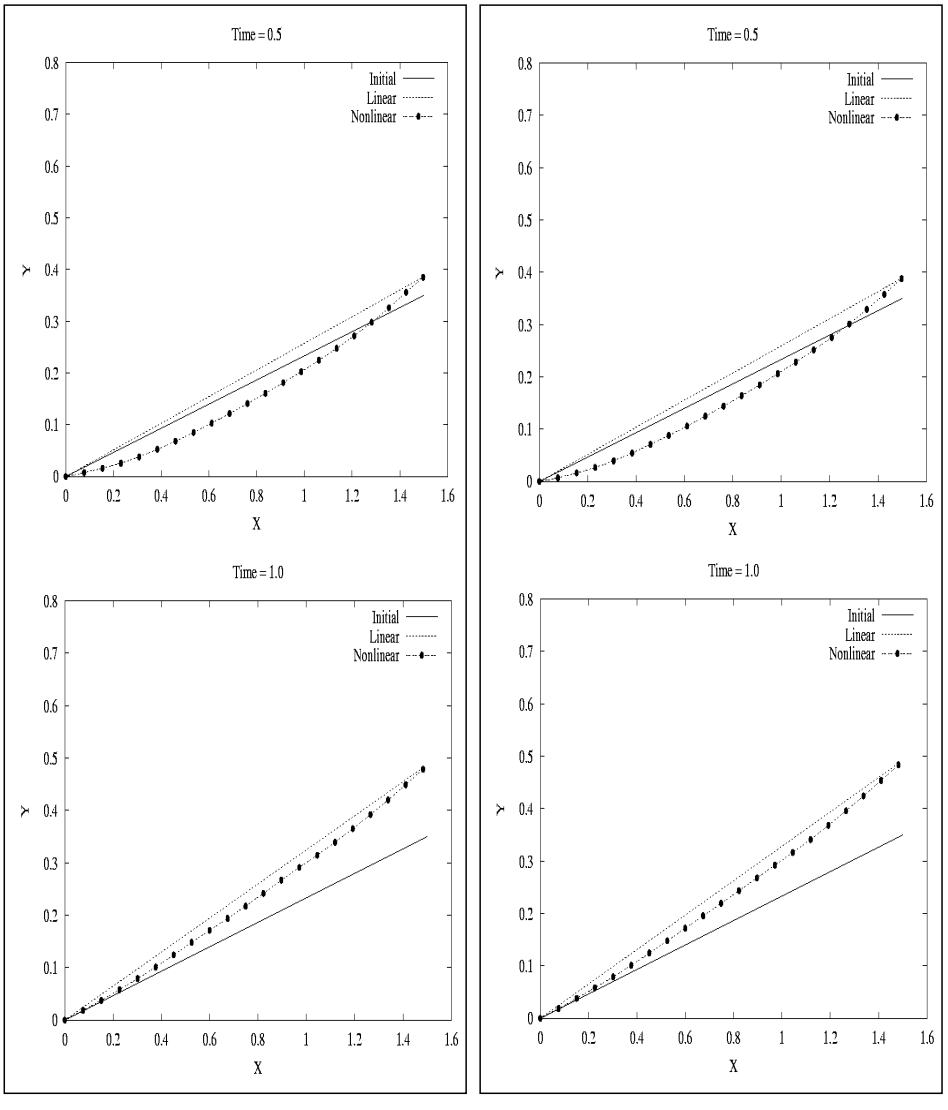

Figure 1. The graphs show the position of the cable at time equal to 0.5 and 1.0. In this figure, the graphs on the left correspond to the solution obtained using the coarse mesh and the graphs on the right correspond to the solution obtained using the fine mesh.

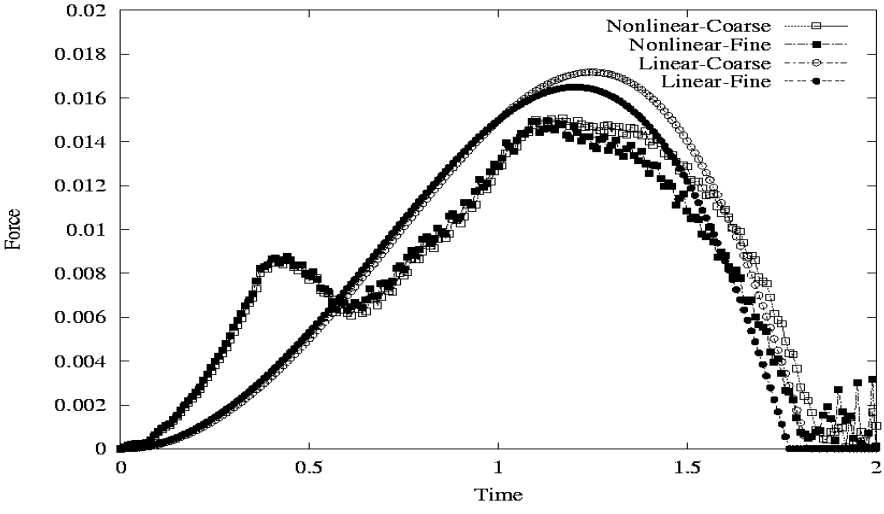

Figure 2. The tensional forces for all four solutions versus time.

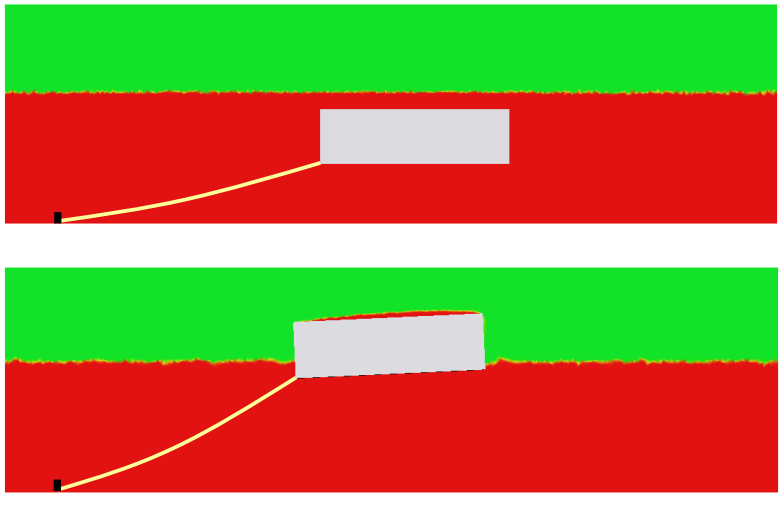

Figure 3. Figure shows the cross section from the computational domain at z = 0.0 and for times at 0.1 (top) and 2.1 (bottom). Here, the color shows the water (red) and air (green) for the *Nonlinear-Fine* solution.

5 CONCLUDING REMARKS

We incorporated two mathematical models for cables into our free-surface flow solver with moving mesh capability. The new free-surface flow solver is capable of simulating mooring forces on floating objects. In our approach, the cables act as constrain for the six degrees of freedom nonlinear rigid body dynamics (6DOF). The solutions of the Navier-Stokes equations for two incompressible fluids, the transient scalar equation governing the motion of the interface, the linear elasticity equations for mesh-moving, the linear and nonlinear equations for cables, and the equations for 6DOF are obtained iteratively at every time step. The numerical example included 3D simulations of floating object constrained with a light-weight cable.

6 ACKNOWLEDGEMENT

Work funded in part by the Army High Performance Computing Research Center under the auspices of the Department of the Army, Army Research Laboratory contract number DAAD19-01-2-0014. Partial support for this publication made possible through support provided by DoD High Performance Computing Modernization Program (HPCMP) Programming Environment & Training (PET) activities through Mississippi State University under the terms of Agreement No. # GS04T01BFC0060. Views, opinions, and/or findings contained in this report are those of the author(s) and should not be construed as an official Department of the Army and Department of Defense position, policy, or decision unless so designated by other official documentation and no official endorsement should be inferred.

7 REFERENCES

[1] B. S. Rosen and J. P. Laiosa, "SPLASH Nonlinear and Unsteady Free-Surface Analysis Code for Grand Prix Yacht Racing", *The Thirteenth Chesapeake Sailing Yacht Symposium,* Annapolis, MD, Jan. (1997).

[2] S. Aliabadi and T. Tezduyar, "Stabilized-Finite-Element/Interface-Capturing Technique for Parallel Computation of Unsteady Flows with Interfaces", *Computer Methods in Applied Mechanics and Engineering*, **190**, 243-261 (2000).

[3] T. Sundel, "Computation of the Free-Surface Flows Around a Ship Using NS Solver FINFLO", VTT Manufacturing Technology, (1997).

[4] S. K. Aliabadi and T.E. Tezduyar, "Space-time Finite Element Computation of Compressible Flows Involving Moving Boundaries and Interfaces", *Computer Methods in Applied Mechanics and Engineering*, **107**, 209-223 (1993).

[5] T.J.R Hughes and G.M. Hulbert, "Space-Time Finite Element Methods for Elastodynamics: Formulations and Error Estimates", *Computer Methods in Applied Mechanics and Engineering*, **66**, 339-363 (1998).

[6] J. Donea, "An Arbitrary Lagrangian-Eulerian Finite Element Method for Transient Fluid-Structure Interactions", *Computational Mechanics*, **33**, 689-723 (1982).

[7] C. Farhat, M. Lesoinne and N. Maman, "Mixed Explicit/Implicit Time Integration of Coupled Aeroelastic Problems: Three-Field Formulation, Geometric Conservation and

Distributed Solution", *International Journal for the Numerical Methods in Fluids*, **21**, 807-835 (1995).

[8] A. Johnson and T. Tezduyar, "Advanced Mesh Generation and Update Methods for 3D Flow Simulations", *Computational Mechanics*, **23**,130-143 (1999).

[9] W. Hirt and B. D. Nichols, "Volume of Fluid (VOF) Method for the Dynamics of Free Boundaries", *Journal of Computational Physics*, **39,**201-225 (1981).

[10] M. Sussman, P. Smareka and S. Osher, "A level Set Approach for Computing Incompressible Two-Phase Flows", Journal of Computational Physics, **114**, 146-168, (1994).

[11] J. A. Sethian, "Level Set Method", *Cambridge Monographs On Applied and Computational Mathematics*, Cambridge University Press, (1996).

[12] Shahrouz Aliabadi, Andrew Johnson, Bruce Zellars, Ade Abatan, and Charlie Berger, "Parallel Simulation of Flows in Open Channels", *Journal of Future Generation Computer Systems*, **18**, 627-637 (2002).

[13] S. Aliabadi and S. Shujaee, "Free Surface Flow Simulations Using Parallel Finite Element Method", *Simulation*, **76**, 257-262 (2001).

[14] A. Johnson and S. Aliabadi, "Application of Automatic Mesh Generation and Mesh Multiplication Techniques to Very Large Scale Free-Surface Flow Simulations", *Proceeding of the 7th International Conference on Numerical Grid Generation in Computational Field Simulations,* Whistler, British Columbia, Canada, September (2000).

[15] S. Aliabadi, A. Johnson, J. Abedi, K. Bota and B. Zellars, "Finite Element Simulation of Hydrodynamics Problems Using Unstructured Meshes with more than One Billion Elements", Proceedings of 8th International Conference on Numerical Grid Generation in Computational Field Simulations, Honolulu, Hawaii, June 2-6, (2002).

[16] S. Aliabadi, B. Zellars, J. Abedi, A. Johnson, C. Berger and J. Smith, "Implicit, Large-Scale, Parallel 3D Simulations of Waves Impacting on Floating Vessels", *Proceedings of the LACSI 2001 Symposium*, Los Alamos National Laboratory, October 16-17, (2001).

[17] S. Aliabadi, J. Abedi, B. Zellars and K. Bota "New Finite Element Technique for Simulation of Wave-Object Interaction", AIAA Paper 2002-0876 (2002).

[18] S. Aliabadi and T. Tezduyar, "Parallel Fluid Dynamics Computations in Aerospace Applications", *International Journal for the Numerical Methods in Fluids*, **21,**783-805 (1995).

[19] T. J. R. Hughes and A. N. Brooks, "A multi-dimensional upwind scheme with no crosswind diffusion", in T. R. Hughes, editor, *Finite Element Methods for Convection Dominated Flows*, ASME, New York, **34**, 19-35, (1979).

[20] G. Gruttmann and R. T. Taylor, "Theory and Finite Element Formulation of Rubber like Membrane Shells Using Principal Stretches", *International Journal for Numerical Methods in Engineering*, **35**, 1111-1126 (1992).

[21] Y. Saad and M. Schultz, "GMRES: Generalized Minimal Residual Algorithm for Solving Nonsymmetic linear Systems", *SIAM Journal of Scientific and Statistical Computing*, **7**, 856-896, (1986).